

Provided for non-commercial research and education use.
Not for reproduction, distribution or commercial use.

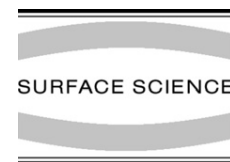


This article was published in an Elsevier journal. The attached copy is furnished to the author for non-commercial research and education use, including for instruction at the author's institution, sharing with colleagues and providing to institution administration.

Other uses, including reproduction and distribution, or selling or licensing copies, or posting to personal, institutional or third party websites are prohibited.

In most cases authors are permitted to post their version of the article (e.g. in Word or Tex form) to their personal website or institutional repository. Authors requiring further information regarding Elsevier's archiving and manuscript policies are encouraged to visit:

<http://www.elsevier.com/copyright>



A numerical approach to quantify self-ordering among self-organized nanostructures

F. Ratto^a, T.W. Johnston^a, S. Heun^b, F. Rosei^{a,*}

^a INRS Energie, Matériaux et Télécommunications, Université du Québec, 1650 Boul. Lionel Boulet, J3X 1S2 Varennes (QC), Canada

^b NEST CNR-INFM and Scuola Normale Superiore, Piazza dei Cavalieri 7, 56126 Pisa, Italy

Received 14 August 2007; accepted for publication 9 October 2007

Available online 25 October 2007

Abstract

The geometrical layout in two-dimensional arrays of self-organized nanostructures is usually not completely ordered, nor completely disordered. The ability to quantify a degree of order gives significant insight in nanoscale self-organization processes. We address this issue analytically. We first simulate the arrangement of nuclei in two-dimensional lattices with mixed order/disorder, as defined by a suitable order parameter. We focus on statistical properties of the local environment of the simulated nuclei. Finally, we compare this statistical analysis with results from actual experimental images. Here we test our analysis with the Ge/Si(111) model system. Our approach reveals a significant tendency towards self-ordering in this system, which is primarily attributed to *Brownian* nucleation and capture dynamics.

© 2007 Elsevier B.V. All rights reserved.

Keywords: Growth; Semiconductor–semiconductor heterostructures; Silicon–germanium; Nanostructures; Nucleation; Monte Carlo simulations; *In situ* characterization; Low-energy electron microscopy (LEEM)

1. Introduction

The self-organization of nanostructures at surfaces represents a phenomenon of fundamental interest in materials science, with great potential in various fields of technology [1,2]. These processes are met in different systems, ranging from organic assemblies on metal surfaces to semiconductor heteroepitaxial islands [3,4], which may yet exhibit very different fundamental dynamics. One most noticeable example of this class of phenomena is the growth of germanium on silicon surfaces, whereby three-dimensional Ge/Si islands nucleate on a flat wetting layer (WL), following a modified Stranski–Krastanov (SK) mode [5–7]. Below a critical size which depends on the materials involved, individual nanostructures are expected to behave as *artificial atoms* or *quantum dots* [8,9], i.e. to exhibit a discrete spectrum of electronic energy levels. Functional interactions

among coexisting nanostructures might be exploited in complex superstructures thereof, ultimately resulting in *artificial molecules* and *artificial crystals* [9–12]. These in turn have attracted much attention in view of applications in the micro- and opto-electronic fields. To take full advantage of the potential of complex QDs architectures, gaining insight and possibly control over the positioning of epitaxially grown islands is essential. The latter rests among the *still-unresolved* critical issues in the literature of semiconductor self-organized nanostructures [2]. Within this framework the concept of self-ordering plays a key role [2,13,14]. It applies to the spontaneous relationship between a self-organized island site and the surrounding environment.

Upon visual inspection, sets of coexisting nanostructures are typically believed to be positioned at random, or disordered [7,15,16]. Such a superficial approach may be inadequate and even misleading. Nor can diffractive methods be regarded as conclusive, since they emphasize the long-range order rather than the short-range nearest-neighbor order of principal interest. To gain an understanding of inter-particle,

* Corresponding author.

E-mail address: rosei@emt.inrs.ca (F. Rosei).

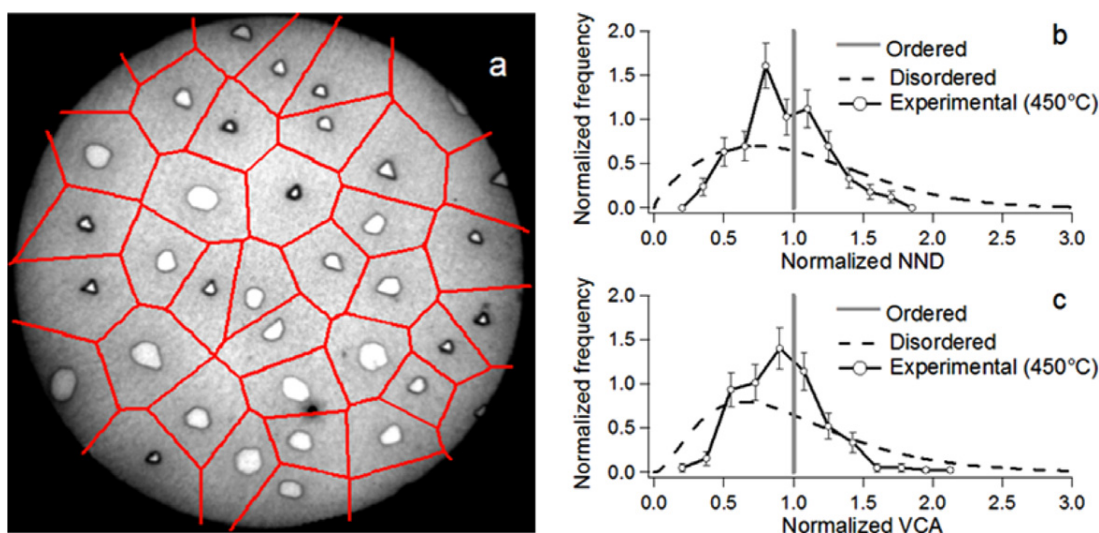


Fig. 1. (a) Ten microliters field of view-LEEM micrograph of a surface obtained by deposition of 10 mono-layers (ML) Ge/Si(111) at 450 °C. (b) Distribution of the nearest-neighbor distances (NND) expected from a perfectly ordered array of islands (dark grey delta function); from a completely disordered arrangement (black dotted line); and measured from experimental micrographs as in (a) (about 500 nanostructures). (c) Same as (b) for the Voronoi cell areas (VCA) distribution.

possibly short-range interactions at play in the formation of islands, the focus of the analysis should be on very *local* properties of their environment (in a local autocorrelation-like approach), including the mixture of order and disorder at the local scale.

To illustrate these concepts in a concrete example, in Fig. 1a we show a typical micrograph (here a 10 μm field of view-low energy electron microscopy (LEEM) image) of Ge/Si(111) nanostructures grown epitaxially at 450 °C on Si(111). In Fig. 1b and c, we plot the relevant distributions of the nearest-neighbor distances (hereafter NND) and Voronoi cell areas (VCA),¹ respectively. (Use of the Voronoi cells with their boundary segments at half the distance between the two neighboring island centers allows a natural cutoff on the number of neighbors, and is convenient to implement numerically.) Clearly these nanostructures are not completely ordered, i.e. they do not rest in a perfect crystalline ‘lattice’. Neither is the system completely disordered. We simulated numerically the NND and VCA distributions from completely Poissonian scatterings of dots (see Fig. 1b and c) and found that such random distributions do not satisfactorily match the experimental results. The experimental results clearly are between the two extremes of complete order and complete disorder, and can thus be fairly described as being at least somewhat *self-ordered*. Here we aim at quantifying this mixture of order and disorder (i.e. the degree of self-ordering) by an approach which deals with the image itself, without appeal to underlying mechanisms.

¹ Voronoi cell areas relate to the Voronoi tessellation of a surface with respect to a given set of *dots*. The Voronoi tessellation is a partition of the surface, whereby each point is associated to the closest possible dot.

We describe a *general-purpose* tool which is meant to quantify the mixing of order and disorder in any given two-dimensional pattern of objects. We devise a simple theory in the broadest possible terms. Our approach is *geometrical* and *numerical* rather than *physical*. We address the following question: Is it possible to measure arbitrarily small, *local* bits of order from micrographs of these objects (generally each separately containing a limited statistics of events as in Fig. 1a)? Depending on the application one may envisage, self-ordering may or may not be desired, and in either case it generally needs to be characterized and quantified thoroughly [15]. Systems of practical interest are in general expected to be a genuine mixture of order and disorder. To set the scene, we give a brief review of the physical reasons *why* some degree of self-ordering might be well expected. The method we propose is then described in detail in Section 3.

2. Some possible factors inducing order

2.1. Role of enthalpic factors

Self-ordering of heteroepitaxial islands could result from enthalpic factors [17–19], originating, e.g. from inhomogeneities in the strain distribution or defect network on the WL. Spontaneous periodic modulations of the strain energy in the WL may appear as surface instabilities leading to wavy morphologies [13,20], such as the Asaro–Tiller–Grinfeld roughening [21–23], with given wavelength [20,24,25]. This may define a correspondingly periodic network of favored nucleation sites [17]. When referring, e.g. to the epitaxy of Ge on Si(111), nanostructures are expected to nucleate preferentially on sites under *tensile* strain.

Other possible enthalpic origins of self-ordering may come from nanostructure–nanostructure interactions, e.g. mediated through the substrate or the WL. In this context island-induced strain fields may play a key role. Strain maps below nanostructures were calculated for Ge/Si(001) [26]. A strong compression was found within a ring around the perimeters of the islands, which is a source of repulsive interactions with neighboring islands [27,28].

The capacity of strain fields to promote self-ordering is witnessed in a more complex context. When Ge/Si nanostructures are stacked by recursively depositing Ge and Si, islands progressively gain vertical and lateral order [19,29], which is attributed to the strain configuration inside the layer [30–32]. Similar processes occur during the first stages of capping of Ge/Si islands with Si at high temperatures. The enhanced surface mobility allows for movements of the nanostructures in an ordered array [33], possibly driven by strain minimization. These island–island interactions develop *locally*, which may translate into poor long-range coherence.

We wish to speculate on the possible trend of self-ordering with temperature, were the phenomenon to be driven by these enthalpic interactions. We assume that the ordered array gives the absolute minimum of the surface enthalpy. The degeneracy of the ordered phase is smaller than that of competing disordered phases. At low enough temperatures (say approaching from above the Ge amorphization temperature) a wealth of activation barriers would trap the system in a metastable configuration with *little* or *no* order. At high enough temperatures (e.g. approaching from below the Ge re-evaporation temperature) entropy would govern the nucleation dynamics, thus leading to a disordered phase. Hence order could be achieved within a suitable *intermediate* temperature range only. Under these assumptions we do not expect surfaces grown at different temperatures to be ‘self-similar’. The picture is complicated by concomitant mechanisms which depend strongly on temperature, such as the atomic intermixing of Ge and Si [34], the nucleation of misfit dislocations [35,36] (altering the strain composition [5,25]), and the variation of the island number density and typical individual dimensions (see below). All things considered, temperature would play a significant role in the mixing of order and disorder.

2.2. A Brownian picture of nucleation

Apart from the considerations above, self-ordering of heteroepitaxial nuclei could be expected from the Brownian nature of the nucleation processes [37]. The formation of three-dimensional nanostructures is likely to occur via a sequence of competitive nucleation and capture dynamics, which are mediated through diffusion in an inhomogeneous density of adatoms [38,39].

When the thickness of the wetting layer (WL) exceeds a critical value, preservation of the flat morphology becomes impossible. Further deposition increases the density of mobile adatoms. These tend to condense in three-dimensional

islands, thereby releasing the epitaxial strain, at least *partially*. Nonetheless, nucleation of islands requires some transient super-saturation of adatoms on the WL. The formation of stable nuclei follows from collisions involving a number of adatoms higher than a critical threshold i (an attribute specific to every epitaxial process) [40]. As a consequence (in a Brownian picture of diffusion) the local probability of nucleation grows with a power law of the local density of adatoms, with exponent $i + 1$.

We imagine that one three-dimensional island has nucleated. Upon formation, the stable nucleus begins to expand through a capture mechanism [41,42], which affects the local uniformity of the adatom density. The super-saturation conditions required for nucleation generally become released *locally* [43,44]. The adatom depletion around an existing nucleus is associated to a local decrease in the probability to form any subsequent nucleus. As for its geometrical consequences, this mechanism of a scarcity of very near island neighbors (compared with a purely random distribution) resembles what might be seen as an *effective* repulsion, induced only by entropic and kinetic factors.

The mutual relationships among coexisting islands are uniquely related to the spatial extent of the adatom-denuded regions. In the Brownian framework, these are limited by kinetic factors, such as the adatom diffusion length. Thus temperature defines the length scale in the system. The surface kinetics may be rather complex. In our example, an Arrhenius plot of the Ge/Si(111) nanostructure number density versus growth temperature gives a straight line (see Fig. 2), revealing that composite thermally activated processes intervene in the nucleation dynamics [45].

The island number density follows very closely an Arrhenius behavior (varying over about two orders of magnitude), with a significant deviation only in the upper part of the temperature range investigated, which is attributed to artifacts in the counting process. The *effective* activation energy inferred from the Arrhenius behavior is very high. It is regarded as a linear combination of the activation energy for diffusion plus additional terms related to the stability of the nucleus, according to $E_a \approx (E_i + iE_d)(5/2 + i)^{-1}$ [45]. Here E_i is the work required for

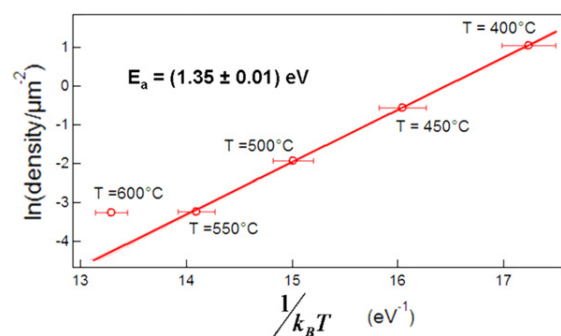


Fig. 2. Arrhenius plot of the island number density. The linear fit is from within the range [400, 550] °C, the data at 600 °C clearly departing from the dominant trend. We report the slope in the plot as an *effective* activation energy E_a .

dissociating the critical nucleus and E_d is the activation energy for diffusion. For comparison, theoretical values of E_d for Ge on the $c(2 \times 8)$ -reconstructed Ge(111) are about 0.8 eV [46]. Our measured $E_a = (1.35 \pm 0.01)$ eV is in excellent agreement with previous findings [45]. Despite the complexity of the phenomena involved, the clear Arrhenius behavior – at least in the range [400, 550] °C – suggests that the bulk of processes underlying nucleation is consistently pictured in a model based on entropy and kinetics only, without the enthalpic factors discussed above. Hence the extent of the adatom-depleted zones could be regarded as dependent solely on an *effective* diffusion length. Under these assumptions, one might well expect that samples grown at different deposition temperatures should be self-similar, i.e. display the same geometrical features except for the typical length scales.

3. Measuring order and disorder: a geometrical approach

The coherence of self-ordering phenomena – either induced by diffusive dynamics or by enthalpic components – may be limited to the short-range [47]. Thus self-ordering should be investigated at the very *local* scale. Here we describe a general-purpose approach, based on the analysis of relative positions of nucleation sites (nearest-neighbors). The experimental data base may be acquired by any imaging technique, even when a small number of nanostructures are seen in each individual image, as in Fig. 1a.

Our approach is to study the distributions of the NND (nearest-neighbor distances) and VCA (Voronoi cell areas) as defined by the arrangement of the nuclei, and using the Voronoi neighborhoods. We will show how the comparison between Monte Carlo (MC) single-step (Brownian-like) displacements of centers from coherently-placed initial sites with experimental data gives a scale for their mixture of order and disorder. We will fit the experimental distributions with results from model systems with: (i) given overall symmetry (chosen from the spatial relationships at play), and (ii) an adjustable degree of order (mixing of order and disorder, as defined below).

The general idea behind our approach is as follows. We want to devise a scale for a useful *order parameter* in systems of experimentally observed particles. We will extract this effective order parameter numerically from a fitting process. In particular, we compare selected aspects of the experimental statistics (measured) with theoretical functions (simulated) containing – as fitting parameter – an effective order parameter (representative of the *degree of order*). The implementation is done numerically by first running MC displacements from an initially ordered lattice with a given degree of order (ratio of the lattice size to the characteristic Brownian step). We extract statistical distributions (NNDs (nearest-neighbor distances) and VCAs (Voronoi cell areas)) from these *simulated* surfaces. These distributions prove to be very well approximated by analytical functions of the order parameter. Finally these functions are compared with the experimental statistics. The

process ultimately yields a *best-fit* order parameter in the real samples. (In fact two values, one from the NNDs and one from the VCAs, whose comparison will give information on the quality of the result.)

We treat the nuclei as zero-dimensional particles scattered throughout a two-dimensional space. We begin by defining a periodic lattice of points, considered as the *perfectly ordered* arrangement of nuclei with the same number density. The generation of partially ordered configurations is next achieved via a displacement of each nucleus from its initial ordered arrangement, basically through a single displacement or re-deposition within some surrounding region of (as opposed to *exactly on*) its initial position. Displacement of each site follows a predefined probability distribution. The average extent of this displacement defines our order parameter as its ratio with the mean inter-centre distance (which is naturally unchanged by the re-distribution). In the following example the initial lattice symmetry chosen is hexagonal, which reflects non-directional interactions. However, the algorithm is not restricted to this type, and can be applied to any lattice.

The probability density function (which integrates to 1 when integrated over $rdrd\phi$) used in the displacement is taken to be azimuthally uniform in polar angle ϕ ($0 \leq \phi < 2\pi$) and as a Gaussian distribution $e^{-r^2/2\sigma^2}/\sigma^2$ in radius ($r \geq 0$) (Formally the angular variation is given as a square pulse in azimuthal angle ϕ of value 1 between 0 and 2π and zero elsewhere as $H(\phi)(1 - H(\phi - 2\pi))$ in terms of the Heaviside step function $H(\phi)$ which is 0 for $\phi < 0$ and 1 for $\phi > 0$.)

$$P_\sigma(r, \phi) \equiv p_\sigma(r)H(\phi)(1 - H(\phi - 2\pi)) \\ = e^{-r^2/2\sigma^2}H(\phi)(1 - H(\phi - 2\pi))/2\pi\sigma^2 \quad (1)$$

Global nucleus displacements are performed simultaneously via MC for all the nuclei, with the same probability function p_σ . Thus σ is the *average* root-mean-square displacement of the nuclei about the ordered positions.

Once a form for p_σ has been selected, the lattice displacement statistics depend uniquely on the parameter σ . When σ approaches zero, the system is perfectly ordered and progressively becomes more and more disordered by increasing σ , up to the limit $\sigma \rightarrow \infty$, whereby the system is entirely disordered (*Poissonian*). Of course, it is really σ/d that defines the order parameter (which must be dimensionless) where d is proportional to the mean inter-centre distance (e.g. the lattice parameter in the ordered configuration). The normalized width σ/d will be used for characterizing the degree of order in the system. Since we would like the order parameter (OP) to approach zero when disorder dominates, we define $OP = d/\sigma$. Obviously we have $OP \rightarrow 0$ for the Poisson distribution, and $OP \rightarrow \infty$ for the perfectly ordered array. We take $d \equiv ((2/3)^{1/2} \langle VCA \rangle)^{1/2}$, wherewith we measure distances hereafter.

The right-hand panels of Fig. 3 display the borders of Voronoi cells resulting from specific MC realizations of hexagonal lattices distorted with decreasing values of OP.

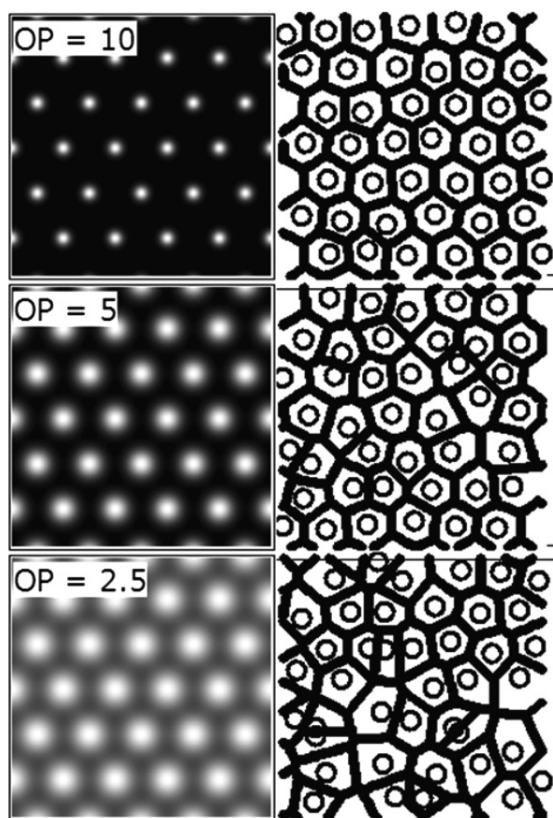


Fig. 3. Probability distribution functions used for generating the distorted lattice (left), together with relevant examples of the MC-simulated positions of the nuclei (right). The right panels also display the boundaries of the Voronoi mosaic.

The left-hand panels show the probability densities used in the simulations (exactly one nucleus per site). It is worth noting how a relatively small displacement from the hexagonal lattice (e.g. $OP = 2.5$) can be easily mistaken on simple visual inspection with a *random* scattering of particles. This kind of mistake may also occur in the analysis of experimental micrographs (e.g. in the heteroepitaxy of semiconductors) [15,48], as suggested by the qualitative similarity between Fig. 1a and the lower right panel of Fig. 3. We will demonstrate that the qualitative correspondence is indeed quantitative as well.

To become quantitative, we define two functions of σ as in the following. Both associate the normal widths σ with functions representing the simulated statistics. We choose the latter as the NND and VCA distributions resulting from a global displacement according to p_σ . Then by fitting experimental data for NND and VCA to these functions (to be defined below), we infer effective values for σ . These are measurements of the mixture of order and disorder.

Using MC simulations similar to those sketched in the right panels of Fig. 3, we have implemented the definition of these functions *numerically*. For any deposition of nuclei with a given value of σ , we have characterized the probability distributions for the NND and for the VCA. To reduce the mathematical complexity, we have fitted these distribu-

tions to explicit and *simple* analytical expressions, containing the smallest possible number of parameters.

All the distributions for the NND can be excellently described by a Weibull expression ($f(x; a, b) = \frac{ax^{a-1}}{b^a} e^{-(x/b)^a}$, $x \rightarrow$ NND; $a, b \rightarrow$ tuning parameters). All the distributions for the VCA can be successfully approximated by a gamma function ($f(x; c, d) = \frac{x^{c-1}}{\Gamma(c)} e^{-(x/d)}$, $x \rightarrow$ VCA; $c, d \rightarrow$ tuning parameters). The latter has already been used to approximate the random limit, as well as random scatterings of points with mutual exclusion zones [49]. When the NND and VCA are normalized to their average values and the relevant frequencies to their integral areas, the simulated distributions can be fitted through the following expressions, each of which depends on only one parameter (either α or β)

$$\begin{aligned} f_{\text{NND}}^\alpha(d) &= \alpha A (Ad)^{\alpha-1} e^{-(Ad)^\alpha}, \text{ with parameter } \alpha \\ &\text{and } A \equiv A(\alpha) = \Gamma(1 + \alpha^{-1}) \\ f_{\text{VCA}}^\beta(S) &= \beta B (\beta S)^{\beta-1} e^{-\beta S}, \text{ with parameter } \beta \\ &\text{and } B \equiv B(\beta) = \Gamma(\beta)^{-1} \end{aligned} \quad (2)$$

This greatly simplifies the original quest to find the best-fit value for σ from the observations of NND or of VCA. First, because of the analytic forms of f_{NND}^α or f_{VCA}^β , it is easy to iterate α or β to find the best-fit value to the data. We also wish to link the α and β values to the corresponding σ through the MC simulations, in order to link the fit to the appropriate σ .

We have performed simulations for different values of the order parameter OP and estimated the relevant best-fit values for α and β . For a typical value for σ , namely $\sigma = 1/4$ (i.e. $OP = 4$), the top panels of Fig. 4 display the fits with f_{NND}^α and f_{VCA}^β of the NND and VCA distributions respectively. Both fits are very satisfactory and properly reproduce the main statistical characteristics of the simulated distributions. Fits similar to those in Fig. 4 were performed for different values of σ . The best-fit for α and β were determined for each of these σ -values and are plotted in the two lower panels of Fig. 4 as $\alpha(\sigma)$ versus σ and $\beta(\sigma)$ versus σ .

Both $\alpha(\sigma)$ and $\beta(\sigma)$ are satisfactorily reproduced by functions derived from parametric sigmoids ($f(x; a, b, c, d) = \frac{a}{b+ce^{-dx}}$) in the $\log(\alpha)$, $\log(\beta)$ - $\log(\sigma)$ space, as given in

$$\begin{aligned} \alpha &= -4.37 + 6.07 \cdot \exp\left(0.475 \cdot (0.325 + 15.8 \cdot \sigma^{2.29})^{-1}\right) \\ \beta &= 0.717 + 1.41 \cdot \exp\left(4.73 \cdot (0.711 + 4.40 \cdot \sigma^{1.20})^{-1}\right) \end{aligned} \quad (3)$$

This analytical expression gives an approach to a constant in the limit $\sigma \rightarrow \infty$ and a power law behavior (straight line in the logarithmic plot) followed by a slight saturation for $\sigma \rightarrow 0$ (see Fig. 4). The first observation is predictable, since the simulated distributions converge to the Poissonian limit for decreasing order. This corresponds to finite values

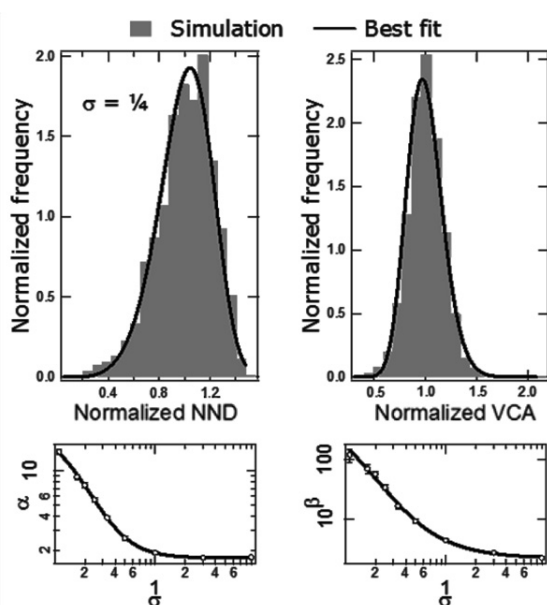


Fig. 4. Upper panels: statistics relative to a simulation performed for $\sigma = 1/4$ together with the best-fits to the Weibull and gamma expressions. The lower panels display the σ -dependence of the parameters α and β used in the approximations.

for α and β , determined as $\alpha(\sigma \rightarrow \infty) = 1.97 \pm 0.09$ and $\beta(\sigma \rightarrow \infty) = 3.49 \pm 0.03$.² The latter compares well with values reported in the literature for a Poissonian distribution, close to $7/2$ [50]. When σ approaches zero, the distributions for the VCA and NND should continuously tend towards δ -like functions, which are actually *not* reproducible by any finite values of α and β . However, the trends as σ tends to zero for α ($\alpha \approx \sigma^{-1}$) and β ($\beta \approx \sigma^{-2}$) are readily understood as expected scaling behavior for function sequences extrapolating to delta functions for, respectively, a one-dimensional distribution such as that representing NND behavior and for a two-dimensional object representing VCA behavior. The limits for α and β we actually reached for lowest σ here are regarded as a simple consequence of the limited resolution of our simulations.³ Our approach is accurate for large distortions and becomes unreliable for very small displacements, where diffraction techniques may be the method of choice. In any case, we do not expect its application for very high OP, say above 10.

Upon identification of proper approximations for $\alpha(\sigma)$ and $\beta(\sigma)$, we define two functions of the Gaussian width σ as:

$$\begin{aligned}
 F_{NND}(\sigma) &= f_{NND}^{\alpha(\sigma)} = \alpha(\sigma) \Gamma(1 + \alpha(\sigma)^{-1})^{\alpha(\sigma)} d^{\alpha(\sigma)-1} \\
 &\quad \times \exp(-(\Gamma(1 + \alpha(\sigma)^{-1})d)^{\alpha(\sigma)}) \\
 F_{VCA}(\sigma) &= f_{VCA}^{\beta(\sigma)} = \beta(\sigma)^{\beta(\sigma)} \Gamma(\beta(\sigma))^{-1} S^{\beta(\sigma)-1} \exp(-\beta(\sigma)S)
 \end{aligned}
 \tag{4}$$

² These values were obtained numerically and may be affected by minor systematic errors stemming from the size of the bins in the histograms.

³ In our case and in our (linear) units the resolution was 0.04 (corresponding to OP = 25).

with α and β as in Eq. (3). These functions are designed to associate with any positive value of σ two distributions, for the normalized NND and for the normalized VCA.

Fig. 5 displays some selected values of these functions, here expressed in terms of the order parameter OP ($\equiv 1/\sigma$), together with the distributions obtained from an independent set of MC simulations for the random scattering of nuclei. Conversely when the value of OP is very high and the random aspect very small, the spread in NND and VCA values becomes small. The interesting condition is for intermediate values of the order parameter, when the distribution of nuclei looks fairly random, but significant clustering around a mean value in fact occurs, and this is just where our experimental results prove to lie. This aspect is seen both in the considerable self-avoidance seen at lower NND or VCA and in the lack of large empty areas at higher NND or VCA. The whole point of our mixed random-coherent site placing is to provide a system of characterizing this intermediate clustering behavior.

Due to the necessarily limited quality of the simulated samples, we will consider any value of OP lower than about one as basically compatible with the random limit. Conversely the precision of the usual discretization of the analysis system limits credible OP values to 10 or less (i.e., for $OP \geq 10$, we may consider the system as completely coherent). Thus when our tool gives OP values between 1 and 10 it can be used to characterize numerically to what *extent* order and disorder compete in a given ensemble of particles. In this context, the OP can be used as a quantitative measure of the efficiency of the ordering effects, e.g. under different experimental conditions.

4. Experimental statistics on Ge/Si(111) nanostructures

In these final sections we capitalize on the tool developed above to give a quantitative answer to the question: “Do self-organized nuclei of three-dimensional islands in the SK epitaxy of Ge/Si(111) exhibit any coherent positioning (which results from a tendency towards *self-ordering*)?”

As a preliminary observation, we note that, due to the symmetry and isotropic character of the Si(111) surface, any self-ordering driving force must prompt a close-packed arrangement of nuclei. We speculate that particle–particle interactions, stemming either from elastic repulsions among nuclei [27,28,51,52], or the Brownian nature of the nucleation dynamics [37,53,54] must be isotropic. Any ordered pattern in the substrate and WL, e.g. a strain modulation [5,21,25,55], or a coherent dislocation network [43,56], cannot induce any superstructure with symmetry other than *hexagonal*. This makes the direct comparison of the experimental statistics with the functions in the example above consistent and noteworthy.

Our experiments were performed by depositing 10 ML Ge from a solid molecular beam source on clean Si(111) surfaces kept at different temperatures, in an *ultra high vacuum* environment (see Ref. [16]). The surface morphology

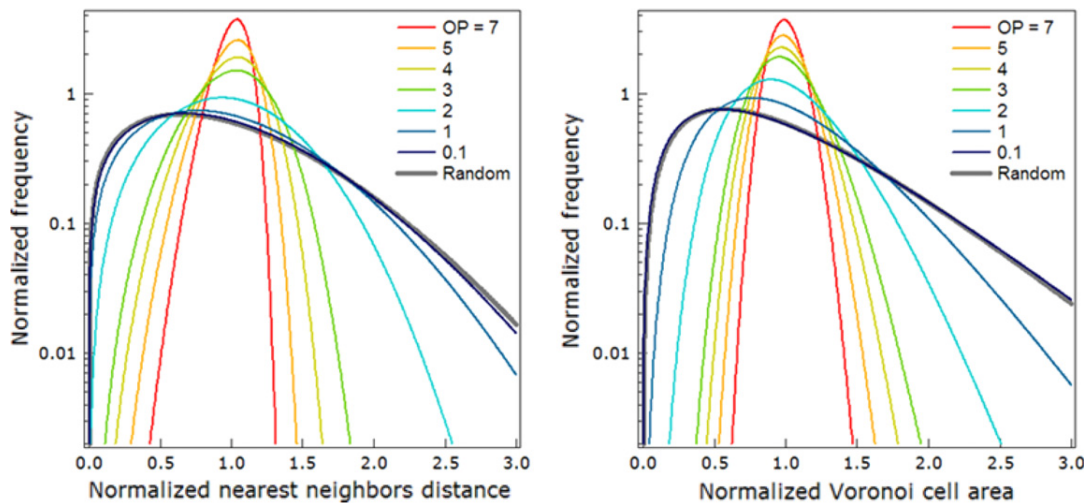


Fig. 5. Examples of the distributions for the NND (left panel) and VCA (right panel), as calculated with F_{NND} and F_{VCA} . The Poissonian limit is also shown for comparison (thick grey line). Note the change in mode, width and skewness of the simulated curves.

was then imaged *in situ* by LEEM with a lateral resolution of ~ 10 nm. Details of the experimental chamber and sample preparation procedure are given elsewhere [16,57,58]. Statistically relevant sets of LEEM micrographs, acquired at different growth temperatures, were used for measuring the NND and VCA statistics. The process is shown in Fig. 1. LEEM microscopy does not allow for a direct measurement of the positions of the nucleation sites of the islands, due to inadequate lateral resolution [59,60]. The information about the surface position of the nuclei is inferred *indirectly* from a set of reasonable assumptions. On the basis of our *dynamic* LEEM observations during growth [16], islands nucleate simultaneously and *initially* grow almost isotropically. In this initial regime they never vanish nor coalesce or merge together. Their majority (apart from a very few percent) follow these conditions up to beyond the investigated coverage range of 10 ML. Under these assumptions, we infer the location of the nucleation sites from the centers of the islands after 10 ML coverage. These are identified accurately (within below 5% of the island–island distance) by LEEM.

Due to the dependence of island number density on growth temperature (Fig. 2), the available statistics was excellent at lower temperatures (up to about 500 islands at 400–500 °C) and more limited at higher temperatures (about 100 islands at 550–600 °C). Average VCA values were used in the plot of the nanostructure number density versus temperature in Fig. 2.

5. Order parameter in ensembles of Ge/Si(111) nuclei

Fig. 6 shows a summary of our results. We have plotted the experimental frequencies of the normalized NND and VCA distributions at different deposition temperatures as thick black ticks (vertical segments placed on the NND and VCA abscissa axes in the left and right-hand panels,

respectively). By visual comparison of the experimental distributions with the simulated random limit (shadowed background curves), it appears that the arrangement of nuclei is inconsistent with a Poissonian distribution of points throughout the temperature range investigated. Significant clustering is indeed clearly evident around the mean values. To quantify a *degree* of order, we use the procedure of Section 3 to fit the measured distributions against the $F_{\text{NND}}(\sigma)$ and $F_{\text{VCA}}(\sigma)$. The appropriate curve for each case is as shown by the various bell-shaped curves in Fig. 6. (The actual OP values obtained are those in Fig. 7 below.)

We emphasize that the set of Eq. (4) contain only *one* fitting parameter each (the width σ). Thus the excellent agreement between the experimental distributions and the model description provides evidence of the merit of our tool.

Fig. 7 reports the best-fitting OP values as a function of deposition temperature. Within the investigated range, the OP is found to lie between 2 and 4, which indicates a *substantial* extent of order. Our figures are inconsistent with a Poissonian scattering of nuclei.

The shadowed band in Fig. 7 was obtained by polynomial interpolation of the data points, and is a guide to the eye only. It was calculated by comparing our two estimates of the OP: from analysis of the NND (systematically higher values) and of the VCA (lower values). With increasing substrate temperatures, the OP possibly exhibits some weak decrease, i.e. order *may* progressively deteriorate. Yet this is well within the experimental error bars. The overall surface statistics seem essentially *unaffected* by the temperature and this despite of a change in the island number density by about two orders of magnitude (see Fig. 2).

The width of the OP band reveals a significant discrepancy between our estimates from the NND and from the VCA. Its breadth is attributed to different possible factors. On one hand the limited experimental statistics may play

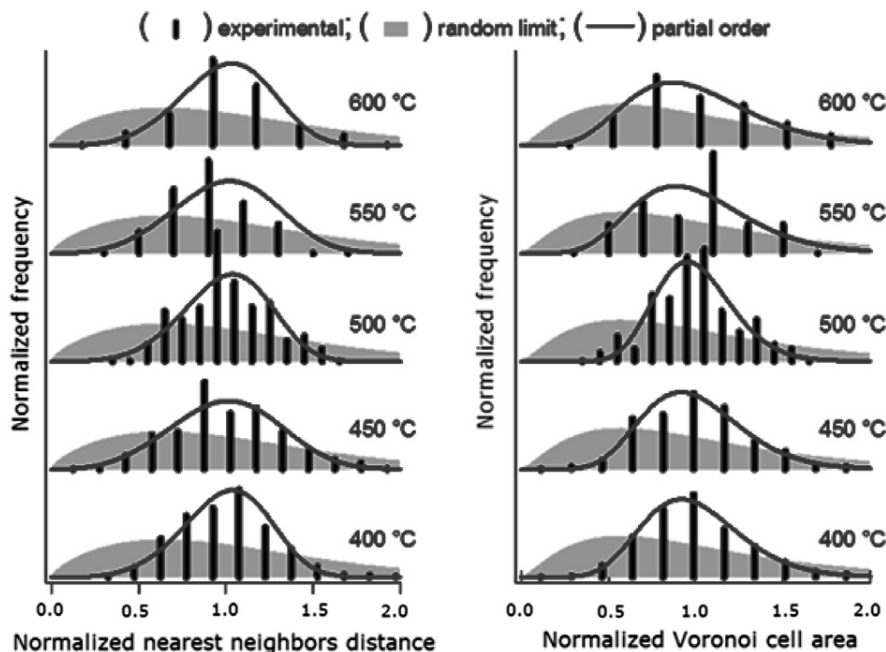


Fig. 6. Comparison between the experimental distributions (black ticks to the abscissa axis), the random MC simulations (shadowed curves), and the best-fits to the functions of σ (bell-shaped lines) for NND (left) and VCA (right).

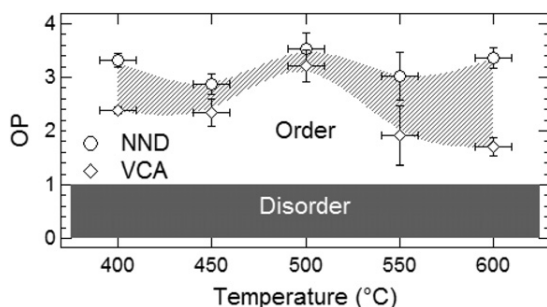


Fig. 7. Order parameter versus substrate temperature, as extracted from the fits of the histograms in Fig. 6. The results from the NND and VCA distributions are reported in the graph as open circles and open squares, respectively. The dark grey shadowed area tentatively marks the boundary between order (un-shadowed) and disorder (shadowed).

an important role.⁴ Indeed the higher the temperature, the lower the island statistics (Fig. 2), and the larger the discrepancy. On the other hand, we speculate that the superposition and convolution of different hexagonal templates may also play a role. In fact ordering may be induced by the competition of processes at different wavelengths and with locally incoherent orientations (which may result e.g. from nucleus–nucleus interactions).

Establishing a relationship between the output of our geometrical analysis and the physical origin of the self-ordering processes is *not* straightforward. However, some useful indications are found in the temperature dependence of OP. Despite evident fluctuations, the observed statistics

are comparable throughout the range investigated, which is consistent with the trend expected from a Brownian picture of nucleation [37].

Here we suggest a possible concept, in qualitative agreement with our experimental findings. The factor primarily governing the relative positions of the coexisting nuclei is the Brownian nature of the nucleation dynamics [37,40,61]. These may account for the weak dependence of OP on temperature. However, enthalpic terms may well play a secondary role as well. These include factors such as strain energy gradients in the WL and elastic repulsions among nuclei [27,28,55]. The interplay of these components (vanishing both at very low and at very high temperatures) may result in some modulation of OP, perhaps giving maxima and minima. The competition of ordering dynamics of different origin, and thus wavelength, local orientation and effectiveness would induce geometrical complexity. This could be only approximately described *locally* as a simple, homogeneously-displaced hexagonal lattice. Such a degree of complexity may contribute to the discrepancy between the OP estimated from the NND and from the VCA. Despite this NND vs. VCA discrepancy, our results demonstrate that some self-ordering in fact occurs. For reasons still to be determined, there is little dependence on temperature for the OP values obtained from NND and rather more variation with temperature on the OP values obtained from VCA.

Experimental evidence for diffusion-mediated nucleation processes has been provided for Ge/GaAs by the report of a narrow distribution for the NND [62]. Similar results have been discussed for the InAs/GaAs [63], and Ge/Si(001) [64] SK systems. The report about InAs/GaAs also

⁴ The width of the bins in the histograms is source of minor artefacts in the fits.

contains qualitative mention of partial hexagonal self-ordering. In the Ge/Si(001) example the experimental statistics have been related to random scatterings of nuclei with *exclusion* zones defined as the average lateral dimensions of the islands. According to our findings this conclusion overstates the role of the size of the nanostructures at a given deposition stage. Islands were *dynamically* observed to nucleate almost simultaneously [16,45], and to grow during deposition quasi-isotropically. Thus self-ordering is here mainly an attribute of the nucleation sites. This in turn is perfectly consistent with the implementation and spirit of our method.

The details of the procedure described in this and in previous sections have been optimized to investigate self-ordering of Ge/Si(111) islands. When appropriately adapted to the particular symmetry and nature of the expected interactions, our approach can be applied to a variety of systems. Due to its local character, it is highly sensitive to small tendencies to ordering, independent of any long-range relationship. On the other hand it is unable to probe the overall symmetry of the surface. These makes this study complementary to traditional analyses based on diffractive tools, where the reverse is true.

6. Conclusions and perspectives

In conclusion, we have developed a geometrical framework and numerical MC approach to quantify the mixture of order and disorder in particles scattered on a surface. Based on the analysis of the local environment of individual particles, our paradigm allows one to detect fairly small degrees of order. Our method leads to useful analytical functions as approximations, which can be compared directly with distributions from actual experimental images. These functions contain fitting parameters, which can be readily converted to order parameter values. Their interpretation gives a scale of the effectiveness of the ordering phenomena.

Here we have shown results obtained by simulating partially ordered close-packed systems. The kind of analysis outlined is in principle straightforwardly adjustable for any other type of symmetry, as imposed by the nature of the candidate ordering driving forces. However, given the complexity of anisotropy studies, a topic closer to hand might be to see whether the MC method might be extended in a scalar (i.e., isotropic) fashion by generalizing the MC probability distribution function by multiplication of Eq. (1) e.g. by a factor $(A + Br^2)$ (with an appropriate normalization, i.e. $B \equiv (1 - A)/2\sigma^2$). The objective would be to see if the best-fit for NND and for VCA could be made to be the same. Each simulation would now depend on σ and on A , which would allow some adjustment of the probability distribution function and perhaps lead to a common pair of values for σ and A which might apply for the best-fit for both NND and VCA. Whether one can still have useful approximations with analytic functions would await future

work, but it seems worth looking at in more detail. Also the interpretation of parameters may lose directness.

When applied to the epitaxy of Ge/Si(111), our approach reveals a substantial tendency towards self-ordering, which is not readily detectable by alternative methods. It demonstrates clustering more closely around the mean values than would be the case for purely random placement of nuclei. This occurs with only modest dependence on temperature particularly for the OP values obtained from NND and rather more variation from VCA. This modest variation with temperature is because the dominant effects are due to the Brownian dynamics underlying the nucleation and growth of stable nuclei. We speculate that enthalpic factors may enhance the tendency towards an ordered configuration. This ultimately results in a pattern more complex than the simple displaced hexagonal lattice used in the simulations. A deeper investigation of the balance between Brownian factors and enthalpic components would be desirable, in view of a complete characterization of self-ordering in Ge/Si(111). We suggest that one way this may be achieved is through the investigation of a broader range of growth temperatures.

We expect this work to stimulate the application of our approach to related systems as well, such as e.g. Ge/Si(001). Non-hexagonal substrate templates and non-isotropic diffusion dynamics may complicate the general theoretical description. Conversely they may make the interpretation of the data easier, since given physical interactions may be unequivocally associated with distinct geometrical configurations.

The focus and scope of our analysis has been on fundamental dynamics in the nucleation of SK islands. We hereby conclude with a short comment on the technological impact of our results. With this respect, we estimate that the extent of self-ordering detected could be quite adverse [15]. It may be insufficient for applications where self-organized close-packed arrays of quantum dots could be desirable, particularly for lasers, diodes, or the like [65–68]. At the same time it may still play some significant role in affecting the sites of quantum dots in artificially designed architectures of *artificial* molecules (including quantum cellular automata or quantum computers) [69–73]. Whatever the case may be, the awareness of some natural tendency in the mutual positioning of islands is extremely important. We hope that our results will be helpful in guiding the technological development of applications based on quantum dots.

Acknowledgements

F. Ratto acknowledges the ICCS, FQRNT and FQRNT-MELS (Quebec) for graduate fellowships. F. Rosei acknowledges funding from NSERC of Canada, and salary support from FQRNT and the Canada Research Chairs program. We are very grateful to Drs. A. Locatelli, S. Fontana, S. Kharrazi, S. Ashtaputre, and Prof. S.K. Kulkarni for their help with the acquisition of the experimental data,

which prompted this theoretical analysis. We gratefully acknowledge useful discussions with Profs. M. Tomellini, M. Fanfoni and R. Rosei.

References

- [1] J.H. Zhu, K. Brunner, G. Abstreiter, *Appl. Phys. Lett.* 73 (1998) 620.
- [2] F. Rosei, *J. Phys.: Condens. Mat.* 16 (2004) 1373.
- [3] F. Rosei, M. Schunack, P. Jiang, A. Gourdon, E. Lægsgaard, I. Stensgaard, C. Joachim, F. Besenbacher, *Science* 12 (2002) 328.
- [4] F.M. Ross, R.M. Tromp, M.C. Reuter, *Science* 286 (1999) 1931.
- [5] I. Berbezier, A. Ronda, A. Portavoce, *J. Phys.: Condens. Mat.* 14 (2002) 8283.
- [6] C. Teichert, *Phys. Rep.* 365 (2002) 335.
- [7] N. Motta, *J. Phys.: Condens. Mat.* 14 (2002) 8353.
- [8] R.C. Ashoori, *Nature* 379 (1996) 413.
- [9] J.V. Barth, G. Costantini, K. Kern, *Nature* 437 (2005) 671.
- [10] L. Kouwenhoven, *Science* 268 (1995) 1440.
- [11] J.L. Gray, R. Hull, J.A. Floro, *Appl. Phys. Lett.* 81 (2002) 2445.
- [12] J. Tersoff, C. Teichert, M.G. Lagally, *Phys. Rev. Lett.* 76 (1996) 1675.
- [13] B. Yang, F. Liu, M.G. Lagally, *Phys. Rev. Lett.* 92 (2004) 025502.
- [14] A. Sgarlata, P.D. Szkutnik, A. Balzarotti, N. Motta, F. Rosei, *Appl. Phys. Lett.* 83 (2003) 4002.
- [15] C.V. Cojocaru, F. Ratto, C. Harnagea, A. Pignolet, F. Rosei, *Microelectron. Eng.* 80 (2005) 448.
- [16] F. Ratto, A. Locatelli, S. Fontana, S. Kharrazi, S. Ashtaputre, S.K. Kulkarni, S. Heun, F. Rosei, *Phys. Rev. Lett.* 96 (2006) 096103.
- [17] V.A. Shchukin, N.N. Ledentsov, P.S. Kop'ev, D. Bimberg, *Phys. Rev. Lett.* 75 (1995) 2968.
- [18] M.I. Larsson, *Surf. Sci.* 551 (2004) 69.
- [19] G. Capellini, M. De Seta, C. Spinella, F. Evangelisti, *Appl. Phys. Lett.* 82 (2003) 1772.
- [20] R.M. Tromp, F.M. Ross, M.C. Reuter, *Phys. Rev. Lett.* 84 (2000) 4641.
- [21] P. Muller, A. Saul, *Surf. Sci. Rep.* 54 (2004) 157.
- [22] M.A. Grinfeld, *Sov. Phys. Dokl.* 31 (1986) 831.
- [23] C.H. Lam, C.K. Lee, L.M. Sander, *Phys. Rev. Lett.* 89 (2002) 216102.
- [24] S.W.J. den Brok, J. Morel, *Geophys. Res. Lett.* 28 (2001) 603.
- [25] B.J. Spencer, P.W. Voorhees, J. Tersoff, *Phys. Rev. B* 64 (2001) 235318.
- [26] P. Raiteri, L. Miglio, F. Valentinotti, M. Celino, *Appl. Phys. Lett.* 80 (2002) 3736.
- [27] J.A. Floro, G.A. Lucadamo, E. Chason, L.B. Freund, M. Sinclair, R.D. Twisten, R.Q. Hwang, *Phys. Rev. Lett.* 80 (1998) 4717.
- [28] G. Capellini, M. De Seta, F. Evangelisti, *J. Appl. Phys.* 93 (2003) 291.
- [29] V. Le Thanh, *Physica E* 23 (2004) 401.
- [30] D. Granados, J.M. García, T. Ben, S.I. Molina, *Appl. Phys. Lett.* 86 (2005) 071918.
- [31] T. Schmidt, E. Roventa, T. Clausen, J.I. Flege, G. Alexe, S. Bernstorff, C. Kübel, A. Rosenauer, D. Hommel, J. Falta, *Phys. Rev. B* 72 (2005) 195334.
- [32] K. Brunner, *Rep. Prog. Phys.* 65 (2002) 27.
- [33] G. Capellini, M. De Seta, F. Evangelisti, V.A. Zinovyev, G. Vastola, F. Montalenti, L. Miglio, *Phys. Rev. Lett.* 96 (2006) 106102.
- [34] F. Ratto, G. Costantini, A. Rastelli, O.G. Schmidt, K. Kern, F. Rosei, *J. Exp. Nanosci.* 1 (2006) 279.
- [35] D.C. Houghton, *J. Appl. Phys.* 70 (1991) 2136.
- [36] M. Hammar, F.K. LeGoues, J. Tersoff, M.C. Reuter, R.M. Tromp, *Surf. Sci.* 349 (1996) 129.
- [37] M. Fanfoni, M. Tomellini, *J. Phys.: Condens. Mat.* 17 (2005) R571.
- [38] M. Tomellini, M. Fanfoni, *Curr. Opin. Solid State Mater. Sci.* 5 (2001) 91.
- [39] J.A. Venables, *Surf. Sci.* 299 (1994) 798.
- [40] M. Zinke-Allmang, *Thin Solid Films* 346 (1999) 1.
- [41] J.A. Blackman, P.A. Mulheran, *Comp. Phys. Commun.* 137 (2001) 195.
- [42] S. Pratontep, M. Brinkmann, F. Nüesch, L. Zuppiroli, *Phys. Rev. B* 69 (2004) 165201.
- [43] H.J. Kim, Z.M. Zhao, Y.H. Xie, *Phys. Rev. B* 68 (2003) 205312.
- [44] F.J. Meyer zu Heringdorf, T. Schmidt, S. Heun, R. Hild, P. Zahl, B. Ressel, E. Bauer, M. Horn-von Hoegen, *Phys. Rev. Lett.* 86 (2001) 5088.
- [45] A.A. Shklyayev, M. Shibata, M. Ichikawa, *Surf. Sci.* 416 (1998) 192.
- [46] A. Selloni, N. Takeuchi, E. Tosatti, *Surf. Sci.* 331–333 (1995) 995.
- [47] I. Kegel, T.H. Metzger, J. Peisl, P. Schittenhelm, G. Abstreiter, *Appl. Phys. Lett.* 74 (1999) 2978.
- [48] L. Vescan, *J. Phys.: Condens. Mat.* 14 (2002) 8235.
- [49] M. Brinkmann, S. Graff, F. Biscarini, *Phys. Rev. B* 66 (2002) 165430.
- [50] F. Járαι-Szabó, Z. Néda, 2004. Available from: <cond-mat/0406116>.
- [51] D.E. Jesson, T.P. Munt, V.A. Shchukin, D. Bimberg, *Phys. Rev. B* 69 (2004) 041302.
- [52] M. Stoffel, A. Rastelli, S. Kiravittaya, O.G. Schmidt, *Phys. Rev. B* 72 (2005) 205411.
- [53] J.A. Amar, M.N. Popescu, F. Family, *Phys. Rev. Lett.* 86 (2001) 3092.
- [54] M. Fanfoni, M. Tomellini, B. Marchetti, F. Gonnella, *J. Phys.: Condens. Mat.* 18 (2006) 8093.
- [55] A. Ramasubramaniam, V.B. Shenoy, *J. Eng. Mater. Technol.* 127 (2005) 434.
- [56] V. Poydenot, R. Dujardin, J.L. Rouviere, A. Barski, F. Fournel, *Appl. Phys. Lett.* 85 (2004) 5700.
- [57] F. Ratto, F. Rosei, A. Locatelli, S. Cherifi, S. Fontana, S. Heun, P.D. Szkutnik, A. Sgarlata, M. De Crescenzi, N. Motta, *J. Appl. Phys.* 97 (2005) 043516.
- [58] A. Locatelli, A. Bianco, D. Cocco, S. Cherifi, S. Heun, M. Marsi, M. Pasqualetto, E. Bauer, *J. Phys. IV* 104 (2003) 99.
- [59] T. Schmidt, S. Heun, J. Slezak, J. Diaz, K.C. Prince, G. Lilienkamp, E. Bauer, *Surf. Rev. Lett.* 5 (1998) 1287.
- [60] R. Wichtendahl, R. Fink, H. Kühlenbeck, D. Preikszas, H. Rose, R. Spehr, P. Hartel, W. Engel, R. Schlögl, H.J. Freund, A.M. Bradshaw, G. Lilienkamp, T. Schmidt, E. Bauer, G. Benner, E. Umbach, *Surf. Rev. Lett.* 5 (1998) 1249.
- [61] R.A. Puglisi, G. Nicotra, S. Lombardo, C. Spinella, G. Ammendola, C. Gerardi, *Phys. Rev. B* 71 (2005) 125322.
- [62] Y.N. Yang, Y.S. Luo, J.H. Weaver, *Phys. Rev. B* 46 (1992) 15387.
- [63] J.M. Moison, F. Houzay, F. Barthe, L. Leprince, E. André, O. Vatel, *Appl. Phys. Lett.* 64 (1994) 196.
- [64] B. Cho, T. Schwarz-Selinger, K. Ohmori, D.G. Cahill, *Phys. Rev. B* 66 (2002) 195407.
- [65] S. Fafard, K. Hinzer, S. Raymond, M. Dion, J. McCaffrey, Y. Feng, S. Charbonneau, *Science* 274 (1996) 1350.
- [66] T.R. Nielsen, P. Gartner, F. Jahnke, *Phys. Rev. B* 69 (2004) 235314.
- [67] N.M. Park, T.S. Kim, S.J. Park, *Appl. Phys. Lett.* 78 (2001) 2575.
- [68] L. Pavesi, L. Dal Negro, C. Mazzoleni, G. Franzo, F. Priolo, *Nature* 408 (2000) 440.
- [69] C.S. Lent, P.D. Tougaw, *Proceedings of the IEEE* 85 (1997) 541.
- [70] C.S. Lent, *Science* 288 (2000) 1597.
- [71] V. Cerletti, W.A. Coish, O. Gywat, D. Loss, *Nanotechnology* 16 (2005) R27.
- [72] D. Loss, D.P. Di Vincenzo, *Phys. Rev. A* 57 (1998) 120.
- [73] M. Kroutvar, Y. Ducommun, D. Heiss, M. Bichler, D. Schuh, G. Abstreiter, J.J. Finley, *Nature* 432 (2004) 81.